JOURNAL OF GEOPHYSICAL RESEARCH, VOL. 108, NO. C11, 8016, doi:10.1029/2002JC001410, 2003

Effects of temperature and circulation on the population dynamics of *Calanus finmarchicus* in the Gulf of St. Lawrence and Scotian Shelf: Study with a coupled, three-dimensional hydrodynamic, stage-based life history model

Bruno A. Zakardjian,[1] Jinyu Sheng,[2] Jeffrey A. Runge,[3] Ian McLaren,[4] Stéphane Plourde,[5,6] Keith R. Thompson,[2] and Yves Gratton[7]

Received 27 March 2002; revised 23 January 2003; accepted 28 May 2003; published 4 November 2003.

[1] We developed a physical-biological model for the Gulf of St. Lawrence (GSL) and Scotian Shelf (SS) by coupling a stage-based life-history model of the planktonic copepod *Calanus finmarchicus* to a three-dimensional ocean circulation model. The life-history model consists of 13 morphologically distinct life stages of *C. finmarchicus*, with stage-specific and temperature-dependent molting rates. The model also includes stage-specific vertical distribution and seasonally varying diapause, egg production, and stage-specific mortality rates. The model domain covers the eastern Canadian shelf from 55°W to 72°W and from 39°N to 52°N, including the Gulf of St. Lawrence, Scotian Shelf, and Gulf of Maine. A comparison of a 1-year simulation with observations indicates that the physical-biological model reasonably describes the observed abundance and distribution of *C. finmarchicus* in this region. To determine the effects of ocean circulation in the *C. finmarchicus* population dynamics, we divided the GSL-SS region into eight sub-areas and compared the net fluxes of *C. finmarchicus* across lateral boundaries to the net production in each sub-area. We found that the annual cross-boundary exchange rates constitute from <1% to 39% of the local net production, indicating that the horizontal transport of *C. finmarchicus* by the ocean currents can play a very important role in the dynamics of local *C. finmarchicus* populations. The results provide insights into the mechanisms of exchange in the GSL-SS system, as put forward in recent hypotheses. *INDEX TERMS:* 4855 Oceanography: Biological and Chemical: Plankton; 4532 Oceanography: Physical: General circulation; 4255 Oceanography: General: Numerical modeling; *KEYWORDS: Calanus finmarchicus*, GLOBEC, hydrodynamic model, life-cycle model, Gulf of St. Lawrence, Scotian Shelf

Citation: Zakardjian, B. A., J. Sheng, J. A. Runge, I. McLaren, S. Plourde, K. R. Thompson, and Y. Gratton, Effects of temperature and circulation on the population dynamics of *Calanus finmarchicus* in the Gulf of St. Lawrence and Scotian Shelf: Study with a coupled, three-dimensional hydrodynamic, stage-based life history model, *J. Geophys. Res.*, *108*(C11), 8016, doi:10.1029/2002JC001410, 2003.

1. Introduction

[2] *Calanus finmarchicus* is a dominant zooplankton species in the North Atlantic Ocean [e.g., *Marshall and Orr*, 1955; *Colebrook*, 1982; *Planque et al.*, 1997; *Planque and Batten*, 2000] and its adjacent seas including the Gulf of St. Lawrence and Scotian Shelf [*Tremblay and Roff*, 1983; *Runge and Simard*, 1990; *de Lafontaine et al.*, 1991]. It is an important prey for early life stages of several commercially important fish stocks, mainly cod and redfish, both in the eastern [e.g., *Hansen et al.*, 1994; *Fossum and Ellertsen*, 1994] and western North Atlantic [*Anderson*, 1994; *Albikovskaya and Gerasimova*, 1993; *Sameoto et al.*, 1994; *Runge and de Lafontaine*, 1996]. The population dynamics of *C. finmarchicus* are greatly affected by ocean currents that may transport it from the deep North Atlantic, where it over-winters at depth, to the relatively shallow shelf regions [e.g., *Backhaus et al.*, 1994; *Aksnes and Blindheim*, 1996; *Slagstad and Tande*, 1996; *Bryant et al.*, 1998; *Gaard*, 1999,

[1]Institut des Sciences de la Mer de Rimouski (ISMER), Université du Québec à Rimouski, Rimouski, Quebec, Canada.
[2]Department of Oceanography, Dalhousie University, Halifax, Nova Scotia, Canada.
[3]Ocean Process Analysis Laboratory, University of New Hampshire, Durham, New Hampshire, USA.
[4]Department of Biology, Dalhousie University, Halifax, Nova Scotia, Canada.
[5]Département de Biologie, Université Laval, Sainte-Foy, Quebec, Canada.
[6]Now at Fisheries and Ocean Canada, Maurice Lamontagne Institute, Mont-Joli, Quebec, Canada.
[7]INRS-Eau, Sainte-Foy, Quebec, Canada.

0148-0227/03/2002JC001410$09.00

2000; *Pedersen et al.*, 2001]. Copepod production may act as a link between hydrodynamic effects of climatic variability and fisheries productivity [*Cushing*, 1984; *Runge*, 1988; *Anderson*, 1994; *Hansen et al.*, 1994; *Skreslet*, 1997; *Runge et al.*, 1999; *Sundby*, 2001]. Because of this potential for physical-biological linkage, *C. finmarchicus* was identified as one of the key species in Global Ocean Ecosystems Dynamics (GLOBEC) research programs for the North Atlantic, including U.S. GLOBEC [e.g., *Wiebe et al.*, 1996], the Trans-Atlantic Study of *Calanus* [*Tande and Miller*, 2000], and GLOBEC-Canada [*Mackas and deYoung*, 2001], all with a major focus on interactions between circulation and *C. finmarchicus* population dynamics.

[3] The Atlantic component of GLOBEC-Canada examined the role of circulation and temperature on the distribution and abundance of *C. finmarchicus* in eastern Canadian waters, in particular the Gulf of St. Lawrence (hereinafter GSL) and Scotian Shelf (SS). Variations in circulation and other environmental features, such as temperature and surface winds, influence the distribution and abundance of zooplankton, notably *C. finmarchicus* [*Runge*, 1988; *Herman et al.*, 1991; *Sameoto et al.* 1994; *Runge and Simard*, 1990; *Head et al.*, 1999]. Geographically, the GSL-SS can be considered as an extended estuarine shelf system under the influence of the freshwater discharge from the St. Lawrence River watershed. The inshore and offshore branches of the Labrador Current and the north-bound of the Gulf Stream also play an important role in controlling its circulation. *Plourde and Runge* [1993] hypothesized that the Lower Estuary acts as a zooplankton "pump," supplying young individuals to the summer population of *Calanus* in the Gulf of St. Lawrence. Transport from the Gulf of St. Lawrence, in turn, was thought to be the dominant source of zooplankton to the Scotian Shelf [*Herman et al.*, 1991], although more recent observations implicate an important role of immigration from the slope water offshore [*Head et al.*, 1999].

[4] As part of the GLOBEC-Canada program, we developed a physical-biological model for the GSL-SS (Figure 1) system by linking a three-dimensional (3D) ocean circulation model (CANDIE [*Sheng*, 2001; *Sheng et al.*, 1998, 2001; J. Sheng et al., Seasonal mean circulation over the eastern Canadian shelf, with emphasis on the Gulf of St. Lawrence and Scotian Shelf, manuscript in revision for *Journal of Geophysical Research*, 2003 (hereinafter referred to as Sheng et al., manuscript in revision, 2003]) that predicts regional temperature, salinity, and flow to a seasonal life-history model of *C. finmarchicus*. Our main objective is to determine how *C. finmarchicus* maintains itself in the extended shelf system given the strong, seasonal variations in the large-scale hydrography and circulation. To what extent does the estuarine advective flow distribute *C. finmarchicus* among regions of the shelf system? What are the major sources and sinks for the population within this advective regime? The model and the results we describe here are directed toward answering these questions through a "climatological run" covering an annual cycle with both realistic regional circulation and *C. finmarchicus* abundance and stage-structure for the GSL-SS region. We present the physical-biological model in section 2. The model results are described in section 3. In this section, we compare the model results to observed

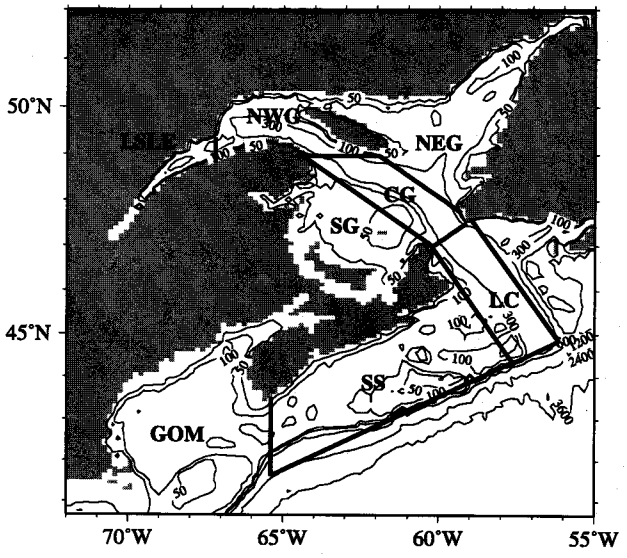

Figure 1. Locations and bathymetry of the sub-areas discussed in the text: Lower St. Lawrence Estuary (LSLE), northwest Gulf of St. Lawrence (NWG), northeast Gulf (NEG), southern Gulf (SG), central Gulf (CG), Laurentian Channel (LC), Scotian Shelf (SS), and Gulf of Maine (GOM). Boundaries indicate sites of flux calculations.

life history cycles and seasonal abundance patterns in the GSL-SS and we estimate the effects of circulation on the dynamics of local *C. finmarchicus* populations. We discuss the implications and future directions leading from these results in section 4.

2. Model Formulation

[5] Given the main objective or our study, which is to quantify advection-induced mixing of sub-populations in a large-scale system, we use a stage-based model embedded in an Eulerian framework. In an Eulerian approach, the biological rates (development, mortality, reproduction) depend on the local environmental conditions but neglect individual histories. While this approach is less efficient in describing individual growth than individual-based models used in other studies of copepod population dynamics [e.g., *Tande and Slagstad*, 1992; *Miller and Tande*, 1993; *Carlotti and Radach*, 1996; *Miller et al.*, 1998], it does allow easier quantitative description of exchange between sub-populations at regional scale. The stage-based model we developed follows the pioneering work of *Wroblewski* [1982] in a form similar to the model described by *Lynch et al.* [1998] for the life history of *C. finmarchicus* in the Gulf of Maine (GOM). The life-history model comprises the egg, six naupliar (NI to NVI), and six copepodid (CI to CVI) stages of the *C. finmarchicus* life cycle [*Marshall and Orr*, 1955]. Adults (stage CVI) are further divided into males (CVIm) and reproductively immature (CVIfj) and mature females (CVIfm). In addition, the model accounts for mortality and development during the diapausing CV (CVd) stage. The time-varying abundance at each stage (number per cubic meter) is determined by the combined effects of (1) advection, (2) turbulent mixing, (3) stage-specific

vertical distribution and swimming behavior (except eggs), (4) stage-specific and temperature-dependent molting rates, (5) stage-specific, seasonally varying, and temperature-dependent mortality rates, and (6) for eggs, seasonally varying spawning by CVI females. Description of the CANDIE results that set environmental conditions, *C. finmarchicus* life history model and coupling with the CANDIE fields are detailed in the subsequent sections.

2.1. Environmental Conditions: The CANDIE 3D Hydrodynamic Model

[6] The hydrodynamic model used in this study is the 3D nonlinear z-level ocean circulation model known as CANDIE [*Sheng et al.*, 1998]. This model has been subjected to rigorous testing (D. Wright, personal communication, 2002) and successfully applied to various modeling problems on the shelf, which include wind-driven circulation over an idealized coastal canyon [*Sheng et al.*, 1998], nonlinear dynamics of the Gaspé Current [*Sheng*, 2001], tidal circulation in the GSL [*Lu et al.*, 2001], seasonal circulation over the northwest Atlantic Ocean [*Sheng et al.*, 2001], and most recently, seasonal circulation in the western Caribbean Sea [*Sheng and Tang*, 2003]. In the present study, CANDIE was applied to the eastern Canadian shelf between 55°W and 72°W and between 41°N and 52°N (Figure 1). The model horizontal resolution is about 13 km in longitude and 9 km in latitude. There are 21 unevenly spaced z-levels in the vertical, with higher resolution near the surface.

[7] CANDIE was run in diagnostic mode with the model temperature and salinity at each time step interpolated linearly from the two nearest values for the seasonal-mean climatology (Sheng et al., manuscript in revision, 2003). Wind stress was set to zero in the momentum equation, but 12-hourly wind fields with a resolution of 2.5° obtained from the European Centre for Medium-Range Weather Forecasts were used to estimate the surface mixing depth and the vertical mixing coefficients. A time-varying eastward flow was introduced at the head of St. Lawrence Estuary to represent freshwater runoff from the St. Lawrence River. At the model lateral closed boundaries the normal flow and tangential stress of the currents were set to zero (free-slip conditions). Along the model open boundaries, an explicit Orlanski radiation condition [*Orlanski*, 1976] was first used to determine whether the open boundary is passive (outward propagation) or active (inward propagation). If the open boundary is passive, the normal flow at the open boundary is radiated outward to allow any perturbation generated inside the model domain to propagate outward as freely as possible. If the open boundary is active, the normal flow at the open boundary is restored to the seasonal mean climatology at each z-level with the timescale of 15 days. In addition, three steady barotropic jets were specified at the eastern open boundary to simulate the influence of the Labrador Current: one through the Strait of Belle Isle, and the other two near St. Pierre Bank to the south of Newfoundland.

[8] Figure 2 shows the temperature fields at the model's top z-level (centered at 5 m from surface) interpolated from the seasonal mean climatology constructed for the region by Sheng et al. (manuscript in revision, 2003). The near-surface waters in the GSL-SS region are relatively cold and spatially uniform in winter (January to March), and warm up gradually from south to north in spring (April to June). With continuous surface heating, the near-surface temperature in the region reaches its maximum in summer (July to September) and then decreases gradually in fall (October to December). The time-depth distributions of water temperatures in the upper 300 m averaged horizontally over sub-regions (Figure 3) exhibit a gradual establishment of the upper-ocean stratification in spring and summer, and relatively rapid establishment of cold and weakly stratified waters in fall and winter. This is consistent with the fact that the upper ocean in this region has relatively weak vertical mixing in spring and summer from the stable stratification associated with surface heating, but strong convective mixing in fall and winter associated with surface cooling (Sheng et al., manuscript in revision, 2003). The interpolated temperature and salinity fields are characterized as the time evolution from a two-layer system in winter (a cold, relatively fresh surface layer overlying a warmer and saltier bottom layer) to a three-layer system in summer (a warm, relatively fresh surface layer, a cold intermediate layer, and a warmer and saltier bottom layer) in the LSLE and GSL, as described by *Koutitonsky and Bugden* [1991]. The maximum and minimum interpolated temperatures at each z-level also agree reasonably well with the previous estimates in the region [e.g., *Koutitonsky and Bugden*, 1991; *Petrie et al.* 1996]. The model calculated 3D currents reproduce many well-known large-scale circulation features in the region (Figure 4), including a year-round cyclonic gyre over the northwestern GSL, southeastward outflow through the western Cabot Strait, and southwestward flow on the SS with relatively strong coastal and shelf-break jets.

2.2. *C. finmarchicus* Life-History Model

[9] The generic formulation for the abundance of stages NII to CV can be written as equations (1)–(5) in Table 1, where $\vec{U}$ is the 3D velocity vector from the CANDIE model, K_z represents vertical mixing, and the terms in the second set of brackets on the right-hand side represent the biological processes (development, mortality, swimming, etc.). The terms μ_{Ni} and μ_{Ci} represent stage-specific molting rates, m_{Ni} and m_{Ci} are mortality rates, and W_{Ni} or W_{Ci} are vertical swimming speeds of the life stages (here the subscripts N and C represent naupliar and copepodid stages, respectively).

[10] Stage-specific molting rates act as cascading transfer functions from eggs to diapausing CV, adult males and immature females. The molting rates were defined in terms of stage-specific, temperature-dependent development times (Table 2) estimated from laboratory experiments [*Campbell et al.*, 2001b], which differ only slightly from estimates by *McLaren et al.* [1988]. We assume that development time, to stage i(either naupliar or copepodid), has a corresponding stage-specific molting rate $\mu_i = \ln(2)/(D_i - D_{i-1})$. The term $\ln(2)$ in the numerator follows from $(1/C_i)\, dC_i/dt = \mu_i$ and the experimental convention that $\frac{1}{2}$ of the population of stage $i-1$ molts to stage i after the time $(D_i - D_{i-1})$. We tested the ability of this formulation to simulate cohort development in a simple preliminary simulation assuming constant temperature, an initial egg population, no mortality, and sterile adults. Figure 5 shows that the model preserves the initial stock as the cohort matures. Development time to adult is somewhat longer (10–20 days) than predicted by the theoretical

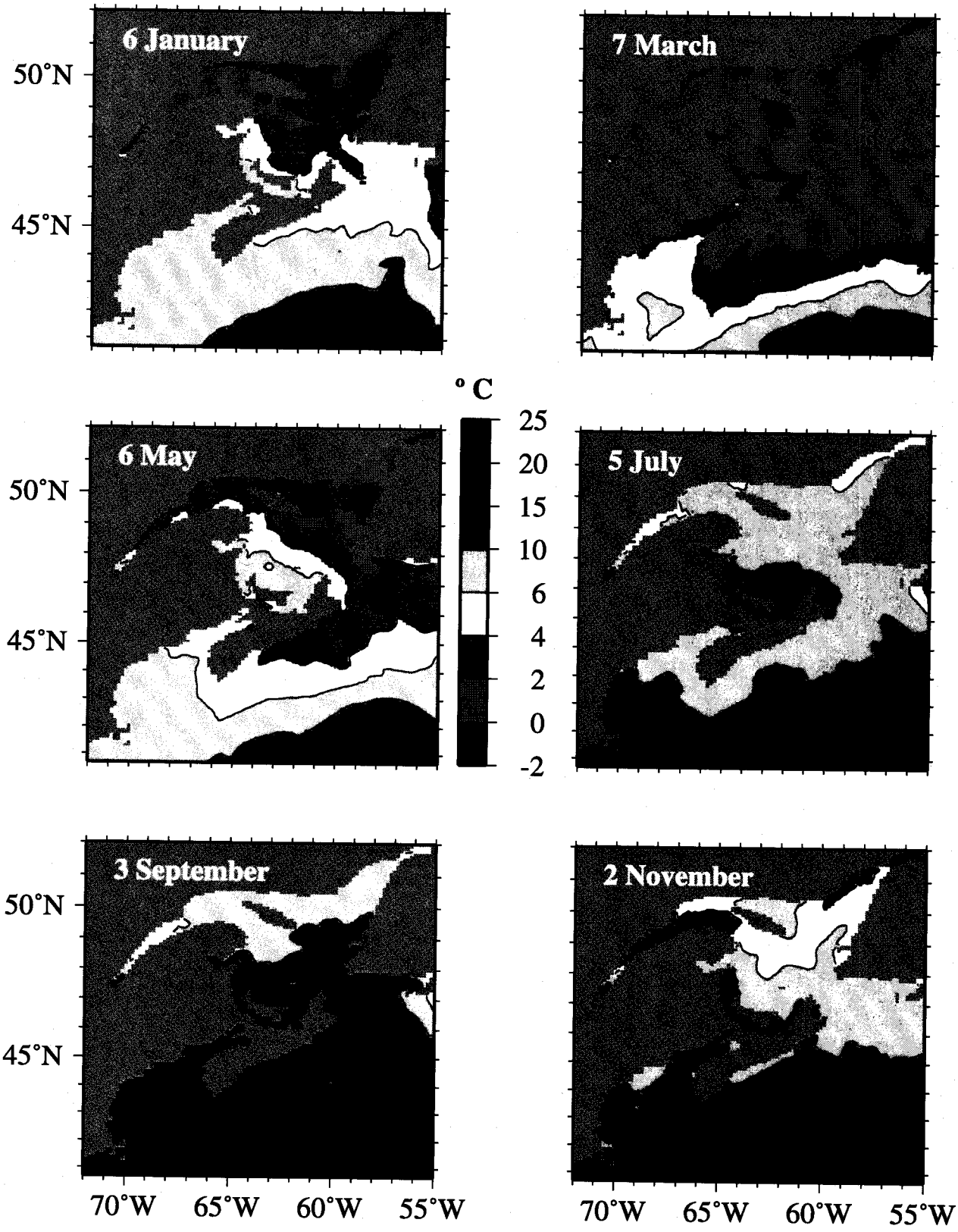

Figure 2. Simulated seasonal patterns of the sea-surface temperature produced by the CANDIE physical model.

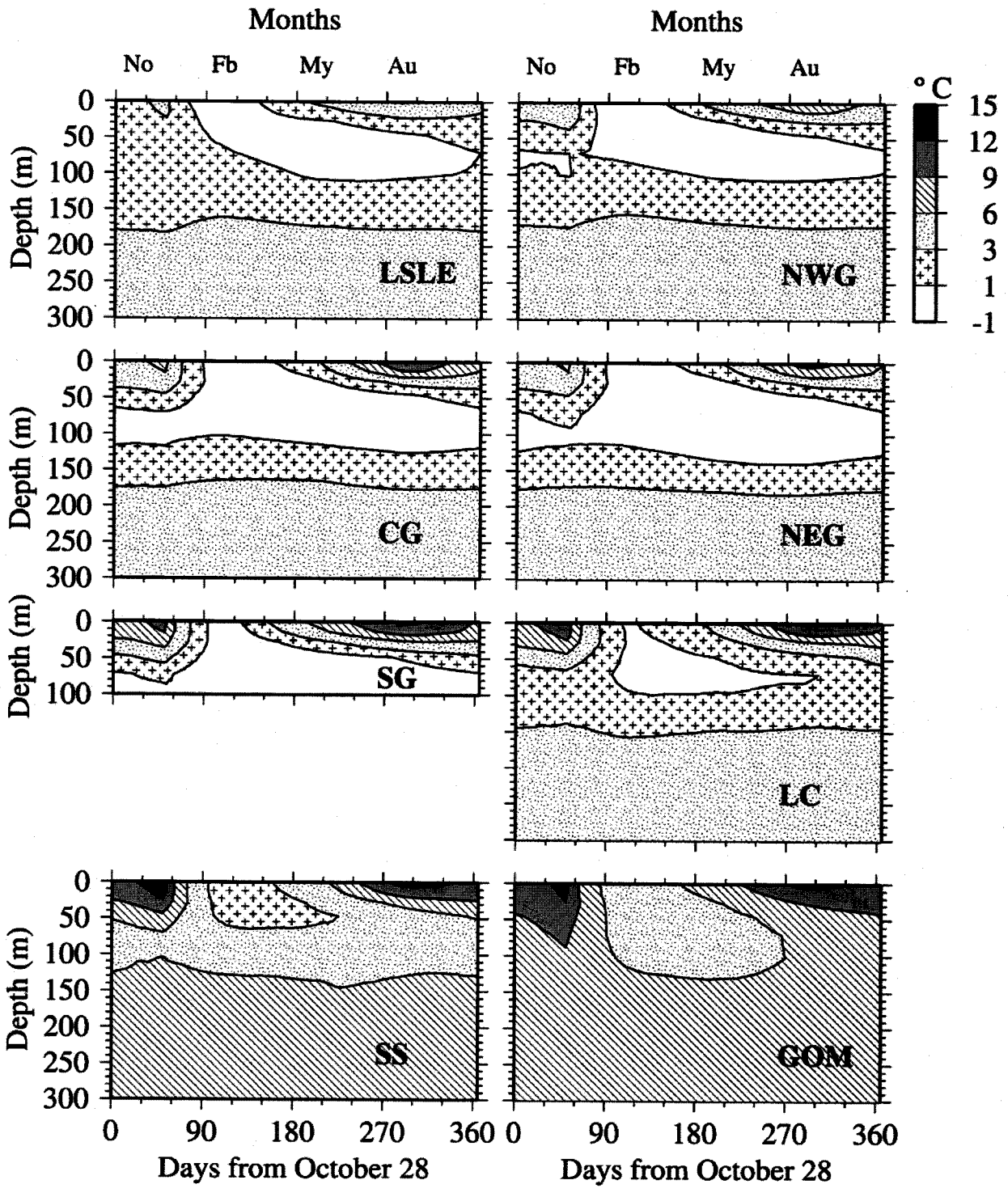

Figure 3. Seasonal trends, as simulated by CANDIE, of the vertical distribution of temperature in the upper 300 m. Regional abbreviations as in Figure 1.

Belehradek function; on the other hand, premature maturation, which is inherent in the Eulerian approach, is less than 20% in all cases.

[11] The governing equations for the abundance of eggs, adults, and CV in diapause are different from the generic equations (1)–(5), in order to include specific biological processes for these stages. First, at the end of their intermolt period, CVs were allocated either to enter diapause or to molt to adult in percentages determined by a seasonally varying function, Diap (equation (11)) where t is time and LagT

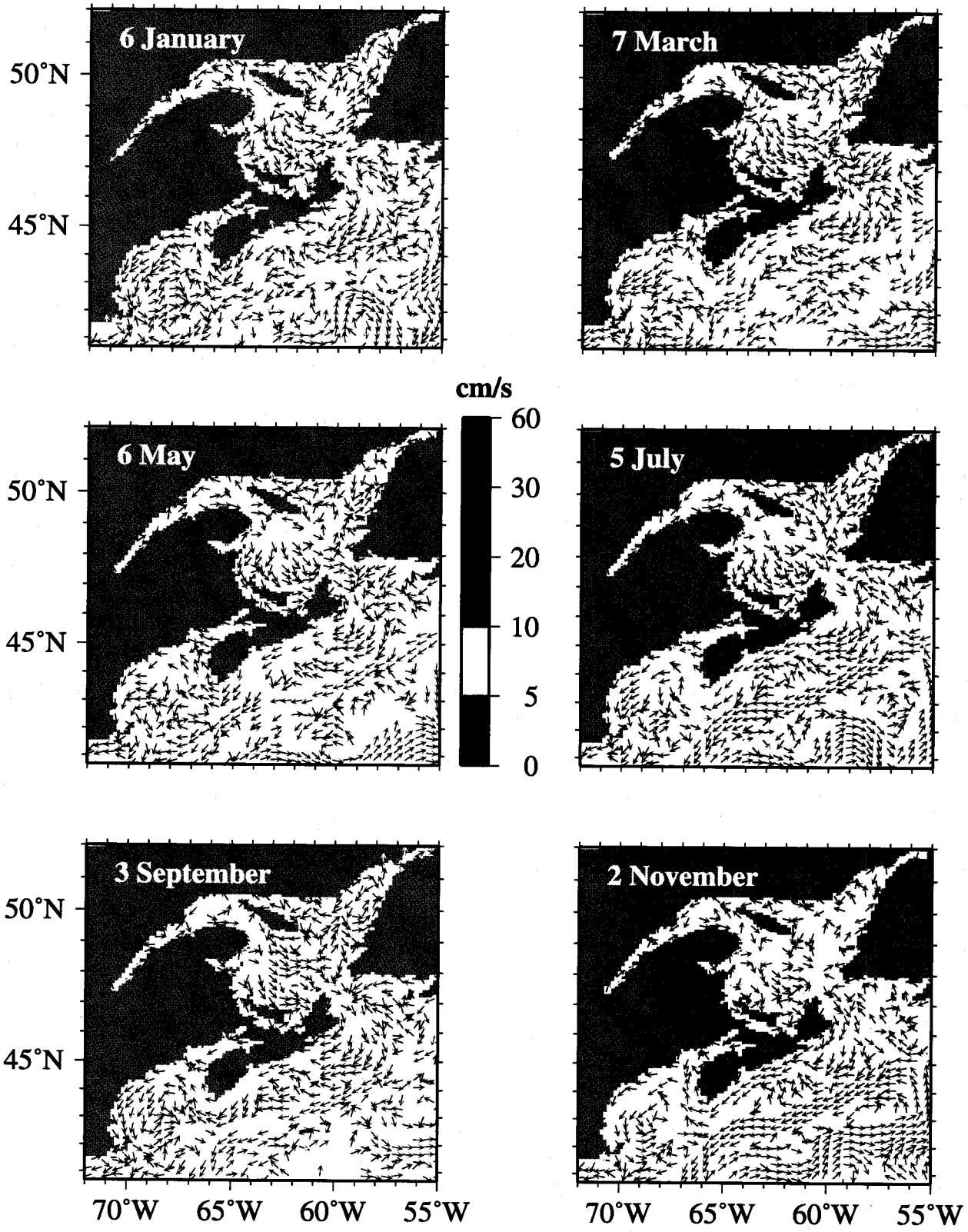

Figure 4. Simulated seasonal patterns of the surface circulation calculated by the CANDIE model. Colors represent current speed.

Table 1. System of Differential Equations and Biological and Climatological Functions Used for the Spatial and Temporal Evolution of the State Variables[a]

Equation	Number
$\frac{\partial}{\partial t}(\mathrm{Eggs}) + \nabla[\vec{U}.\mathrm{Eggs}] = \frac{\partial}{\partial z}\left[K_z \frac{\partial}{\partial z}(\mathrm{Eggs})\right] + \left[-\mu_{\mathrm{Eggs}}.\mathrm{Eggs} + \mathrm{Spawn}.\mathrm{CVIfm} - m_{\mathrm{Eggs}}.\mathrm{Eggs}\right]$	(1)
$\frac{\partial}{\partial t}(\mathrm{NI}) + \nabla[\vec{U}.\mathrm{NI}] = \frac{\partial}{\partial z}\left[K_z \frac{\partial}{\partial z}(\mathrm{NI})\right] + \left[-\mu_{\mathrm{NI}}.\mathrm{NI} + \mu_{\mathrm{Eggs}}.\mathrm{Eggs} - m_{\mathrm{NI}}.\mathrm{NI} + \frac{\partial}{\partial z}(W_{\mathrm{NI}}\mathrm{NI})\right]$	(2)
$\frac{\partial}{\partial t}(\mathrm{NII}) + \nabla[\vec{U}.\mathrm{NII}] = \frac{\partial}{\partial z}\left[K_z \frac{\partial}{\partial z}(\mathrm{NII})\right] + \left[-\mu_{\mathrm{NII}}.\mathrm{NII} + \mu_{\mathrm{NI}}.\mathrm{NI} - m_{\mathrm{NII}}.\mathrm{NII} + \frac{\partial}{\partial z}(W_{\mathrm{NII}}\mathrm{NII})\right]$	(3)
$\frac{\partial}{\partial t}(\mathrm{CI}) + \nabla[\vec{U}.\mathrm{CI}] = \frac{\partial}{\partial z}\left[K_z \frac{\partial}{\partial z}(\mathrm{CI})\right] + \left[-\mu_{\mathrm{CI}}.\mathrm{CI} + \mu_{\mathrm{NVI}}.\mathrm{NVI} - m_{\mathrm{CI}}.\mathrm{CI} + \frac{\partial}{\partial z}(W_{\mathrm{CI}}\mathrm{CI})\right]$	(4)
$\frac{\partial}{\partial t}(\mathrm{CII}) + \nabla[\vec{U}.\mathrm{CII}] = \frac{\partial}{\partial z}\left[K_z \frac{\partial}{\partial z}(\mathrm{CII})\right] + \left[-\mu_{\mathrm{CII}}.\mathrm{CII} + \mu_{\mathrm{CI}}.\mathrm{CI} - m_{\mathrm{CII}}.\mathrm{CII} + \frac{\partial}{\partial z}(W_{\mathrm{CII}}\mathrm{CII})\right]$	(5)
$\frac{\partial}{\partial t}(\mathrm{CVd}) + \nabla[\vec{U}.\mathrm{CVd}] = \frac{\partial}{\partial z}\left[K_z \frac{\partial}{\partial z}(\mathrm{CVd})\right] + \left[-(1-\mathrm{Diap}).\mu_{\mathrm{CVd}}.\mathrm{CVd} + \mathrm{Diap}.\mu_{\mathrm{CV}}.\mathrm{CV} - m_{\mathrm{CVd}}.\mathrm{CVd} + \frac{\partial}{\partial z}(W_{\mathrm{CVd}}\mathrm{CVd})\right]$	(6)
$\frac{\partial}{\partial t}(\mathrm{CV\ Im}) + \nabla[\vec{U}.\mathrm{CV\ Im}] = \frac{\partial}{\partial z}\left[K_z \frac{\partial}{\partial z}(\mathrm{CV\ Im})\right] + \left[\frac{(1-\mathrm{Diap})}{2}[\mu_{\mathrm{CV}}.\mathrm{CV} + \mu_{\mathrm{CVd}}.\mathrm{CVd}] - m_{\mathrm{CVIm}}.\mathrm{CV\ Im} + \frac{\partial}{\partial z}(W_{\mathrm{CV\ Im}}\mathrm{CV\ Im})\right]$	(7)
$\frac{\partial}{\partial t}(\mathrm{CVIfj}) + \nabla[\vec{U}.\mathrm{CVIfj}] = \frac{\partial}{\partial z}\left[K_z \frac{\partial}{\partial z}(\mathrm{CVIfj})\right] + \left[\frac{(1-\mathrm{Diap})}{2}[\mu_{\mathrm{CV}}.\mathrm{CV} + \mu_{\mathrm{CVd}}.\mathrm{CVd}] - \mu_{\mathrm{CVIfj}}.\mathrm{CVIfj} - m_{\mathrm{CVIfj}}.\mathrm{CVIfj} + \frac{\partial}{\partial z}(W_{\mathrm{CVIfj}}\mathrm{CVIfj})\right]$	(8)
$\frac{\partial}{\partial t}(\mathrm{CVIfm}) + \nabla[\vec{U}.\mathrm{CVIfm}] = \frac{\partial}{\partial z}\left[K_z \frac{\partial}{\partial z}(\mathrm{CVIfm})\right] + \left[\mu_{\mathrm{CVIfj}}.\mathrm{CVIfj} - m_{\mathrm{CVIfj}}.\mathrm{CVIfj} + \frac{\partial}{\partial z}(W_{\mathrm{CVIfj}}\mathrm{CVIfj})\right]$	(9)
$m_i(t) = m_i.[1 + \mathrm{Diap}(t)].[1 + (T - 12)/2]$	(10)
$\mathrm{Diap}(t) = 1 - \exp\left[-50[\lvert\sin(\pi(t + \mathrm{LagT})/360)\rvert - 1]^2\right]$	(11)
$\mathrm{Spawn}(t) = [1 - \mathrm{Diap}(t)].\ \mathrm{EPR}_{\max}$	(12)
$W_i = Wm_i \tanh[\alpha(z - Z_i)]$	(13)

[a]Equations for NIII to NVI and CIII to CV are very similar to that of NII (equation (3)) and CII (equation (5)), respectively, and are not detailed further.